CHEMISTRY OF MATERIALS

Article

pubs.acs.org/cm

# Iron Catalysts for the Growth of Carbon Nanofibers: Fe, $Fe_3C$ or Both?

Zhanbing He,*[,†,‡] Jean-Luc Maurice,[†] Aurélien Gohier,[†] Chang Seok Lee,[†] Didier Pribat,*[,§] and Costel Sorin Cojocaru[†]

[†]Laboratoire de Physique des Interfaces et Couches Minces, LPICM, UMR 7647, Ecole Polytechnique-CNRS, Route de Saclay, 91128 Palaiseau Cedex, France

[§]Department of Energy Science, Sungkyunkwan University, Suwon 440-746, Korea

Supporting Information

**ABSTRACT:** Iron is a widely used catalyst for the growth of carbon nanotubes (CNTs) or carbon nanofibers (CNFs) by catalytic chemical vapor deposition. However, both Fe and Fe–C compounds (generally, $Fe_3C$) have been found to catalyze the growth of CNTs/CNFs, and a comparison study of their respective catalytic activities is still missing. Furthermore, the control of the crystal structure of iron-based catalysts, that is $\alpha$-Fe or $Fe_3C$, is still a challenge, which not only obscures our understanding of the growth mechanisms of CNTs/CNFs, but also complicates subsequent procedures, such as the removal of catalysts for better industrial applications. Here, we show a partial control of the phase of iron catalysts ($\alpha$-Fe or $Fe_3C$), obtained by varying the growth temperatures during the synthesis of carbon-based nanofibers/nanotubes in a plasma-enhanced chemical vapor deposition reactor. We also show that the structure of CNFs originating from $Fe_3C$ is bamboo-type, while that of CNFs originating from Fe is not. Moreover, we directly compare the growth rates of carbon-based nanofibers/nanotubes during the same experiments and find that CNFs/CNTs grown by $\alpha$-Fe nanoparticles are longer than CNFs grown from $Fe_3C$ nanoparticles. The influence of the type of catalyst on the growth of CNFs is analyzed and the corresponding possible growth mechanisms, based on the different phases of the catalysts, are discussed.

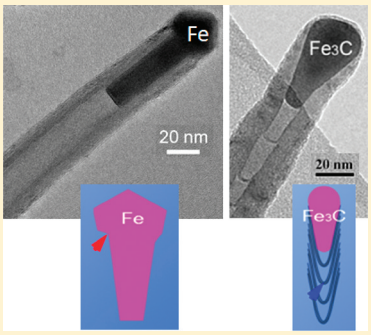


**KEYWORDS:** *carbon nanotubes, carbon nanofibers, PECVD growth, Iron catalyst, α-Fe, $Fe_3C$, growth mechanism, TEM*

## 1. INTRODUCTION

Carbon nanotubes (CNTs)/carbon nanofibers (CNFs) have attracted continuous interest in the past two decades due to their singular properties and their potential applications in the field of nanotechnology. These potentialities have given rise to an intense research activity on catalytic chemical vapor deposition (CCVD) methods, which have been widely studied for large-scale synthesis of CNTs/CNFs.[1] In particular, the plasma-enhanced CVD (PECVD) synthesis process has been developed due to its ability to grow vertically aligned CNTs/CNFs at low temperatures, which is required for applications such as field emission devices.[2,3] Generally, CCVD CNT growth requires transition metal (Ni, Fe, Co) nanoparticle catalysts to decompose a gas mixture based on carbonaceous precursors. However, some crucial questions on the growth mechanisms of CNTs/CNFs by CCVD still generate intense debates, as summarized by Yoshida and co-workers:[4] (1) liquid, solid, or fluctuating structure for catalysts; (2) carbon diffusion through surface or bulk; (3) metal or metal carbide for catalysts. Some experimental or theoretical[4−9] works have been conducted to give some insights on the first two questions, but few experimental works have focused on the crystallographic phases (metal or metal carbide) of catalysts.[4,5]

Concerning iron catalyst, different phases of nanoparticles (e.g., body-centered cubic (BCC) $\alpha$-iron,[10−13] iron carbide,[4,5,10,14−19] and both[20,21]) have been reported from experimental observations. However, few efforts have been made to correlate the nanoparticle chemical nature (e.g., Fe and/or $Fe_3C$) with its catalytic efficiency for CNT growth. Hence, some essential questions about iron-based catalysts for the growth of CNTs/CNFs arise: (1) Are there any differences between the growth mechanisms of CNTs/CNFs, depending on whether the catalyst particles are iron or iron carbide? (2) How do iron or iron carbide affect the growth of CNTs/CNFs? (3) Is it possible to control the crystallographic phases of iron or iron carbide nanoparticle catalysts during growth?

It is of high interest to give some answers to these questions, from both fundamental and technological points of view. In the present paper, by using exactly the same growth conditions with three different growth temperatures, we show that (1) both cementite $Fe_3C$ and $\alpha$-Fe can act as catalysts for the growth of carbon nanotubes/nanofibres, but (2) they are characterized by quite different behaviors: first, only the carbide appears to operate at 600 °C and below; second, the growth rate of CNFs from cementite, $Fe_3C$, appears largely lower than that of CNFs from Fe at higher temperatures (650 and 725 °C). Finally, it is interesting to note that the structure of the nano-objects obtained by Fe and $Fe_3C$ as well as the shape of

**Received:** August 7, 2011
**Revised:** November 10, 2011
**Published:** November 10, 2011

   dx.doi.org/10.1021/cm202315j | *Chem. Mater.* 2011, 23, 5379–5387

the catalysts themselves are different, which can help one to distinguish them easily.

## 2. EXPERIMENTAL DETAILS

**2.1. Growth Conditions.** The vertically aligned CNF arrays were grown from 10 nm thick Fe films deposited on oxidized Si substrates by physical vapor deposition. During the annealing up to the growth temperature and under vacuum, the iron thin film reorganizes to form catalytic seeds (nanoparticles) from which CNFs/CNTs nucleate and grow. Growth was performed by direct current (dc) PECVD using a triode configuration, a method we otherwise develop for field-emission application.[22] Briefly, a dc plasma is generated between two mesh electrodes (anode and cathode) made of graphite. Ions are extracted from the plasma, down to the substrate, by negatively biasing the substrate holder (the third electrode) with respect to the cathode. The growth conditions have been optimized for the fabrication of field emitter arrays; the only parameter that varies here is temperature. The pressure in the reactor is $1 \times 10^{-6}$ mbar before gas introduction and it is set to 2 mbar during growth. The precursor atmosphere is a mixture of water vapor, hydrogen, and isopropyl alcohol with flow rates of 6.5, 3, and 5.5 sccm respectively. These optimized growth conditions correspond to 69% H, 18% C, and 13% O (in at %), so that reducing elements are the major constituents of the plasma. As a consequence, we find little oxygen in the catalyst particles after growth, as shown in Figures S1−3 (Supporting Information), which represent some electron energy-loss spectroscopy (EELS) mapping analysis performed on various carbon fibers after growth, with either Fe (Figures S1 & S2) or $Fe_3C$ catalyst (Figure S3). Only the air-exposed surface of the catalyst particles seems to be slightly oxidized. However, there are at least three phenomenon likely to contribute to the surface oxidation of catalyst particles: (1) oxide formation during the growth of CNFs; (2) iron oxidation (native oxide) during the storage in air and at room temperature for some time; (3) iron oxidation under the electron beam irradiation during the transmission electron microscope (TEM) experiments.[23] We believe that the two latter reasons are likely to be the most important, because the oxygen was found only at the bare surfaces of catalysts and not in the bulk. So, we believe that the weak oxidizing effect of water vapor (and alcohol to a lesser extent) is to suppress the deposition of unwanted amorphous carbon (which would poison catalysts), whereas oxidation of the catalyst particles during growth is prevented by the overall reducing atmosphere inside the reactor. The applied voltage between anode and cathode in the chamber is kept constant at 500 V with a current intensity of 0.2 A. At the beginning of the growth process, the extraction voltage and the extraction current are slowly increased up to the optimum conditions (−50 V; 55 mA). At the end of the process, the chamber is totally pumped out and cooled down. Cooling takes around 30 min without any gas flowing into the chamber. The present CNT synthesis runs were performed at 600, 650, and 725 °C for 36 min.

**2.2. Characterization.** The characterizations of nanotubes/nanofibers and catalysts were performed after the whole growth process was terminated. Of course, only in situ observations of growth would warrant that the shape and structure of the catalysts observed are those that indeed catalyze growth. In the present work, we assume that no phase-change (Fe → $Fe_3C$, or reciprocally) has occurred between growth and observation. This speculation is justified by the present experimental observations (see Discussion).

Scanning electron microscope (SEM) images of CNTs/CNFs were taken by a Hitachi S-4800 FE-SEM with 25 kV accelerating voltage. The TEM samples were prepared by first scratching the deposits on the as-grown samples. CNFs were then adsorbed onto holey amorphous carbon membranes by gently rubbing copper TEM grids on the scratched samples. The TEM images were obtained using a Philips CM 30 instrument working at 300 kV, and a Topcon 002B microscope working at 160 kV. Selected-area electron diffraction patterns (EDPs) were employed to determine the crystallographic phases of catalysts and high-resolution electron microscopy (HREM) images were used to study the microscopic mechanisms involved in the catalytic growth of CNFs. The nanoparticle catalysts were tilted to zone axes to achieve EDPs by using a transmission electron microscope double-tilt specimen holder, which is helpful to distinguish easily the crystallographic phases of $\alpha$-Fe and $Fe_3C$ because of their different lattice parameters, symmetries, and crystal structures.

## 3. RESULTS

Let us first mention that the definitions of carbon nanofiber (CNF) and carbon nanotube (CNT) used here are those proposed by Melechko and co-workers:[2] CNFs are those objects where graphene planes are at an angle with the tube axis (herringbone or bamboo structure) while CNTs are those where these planes are parallel to the tube axis. This generates a qualitative difference for the path of an electric current (e.g., in field-emission applications) traveling along the nanostructure axis: either in the graphene layer plane (tube) or across the graphene planes (fiber). There is a structural continuity between these two kinds of objects and one can decrease the CNF angle (and thus get closer to CNTs) by, e.g., using water vapor in the growth atmosphere.[23]

**3.1. Occurrence of $\alpha$-Fe or $Fe_3C$ Catalysts As a Function of Temperature.** Figure 1 shows the SEM images

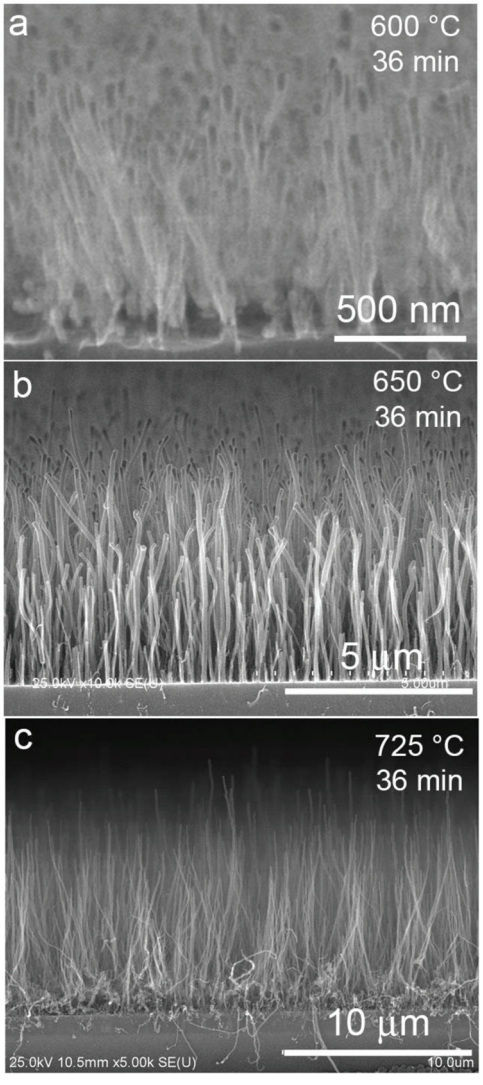


**Figure 1.** SEM images of vertically aligned CNFs grown at different temperatures. (a) 600, (b) 650, and (c) 725 °C. Catalyst nanoparticles appear with a dark contrast at the tips of CNFs.


dx.doi.org/10.1021/cm202315j | Chem. Mater. 2011, 23, 5379–5387

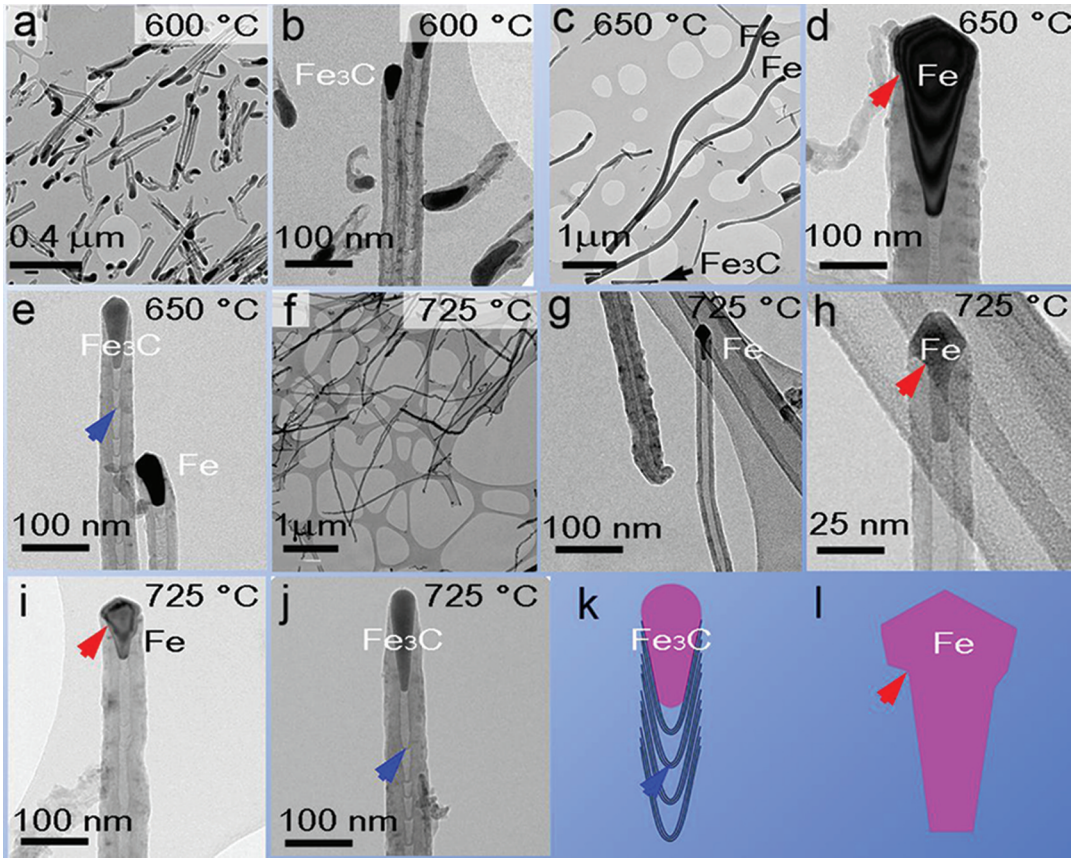


**Figure 2.** Low-magnification and enlarged bright-field TEM images of CNFs/CNTs grown at different temperatures: (a, b) 600, (c–e) 650, and (f–j) 725 °C. (k, l) Schematics of $Fe_3C$ and Fe catalyst shapes. Both $Fe_3C$ and Fe catalysts are elongated along the axis of the tubes/fibers, but the $Fe_3C$ particles exhibit a rounded growth front which contrasts with the faceted one of the Fe particles. Note that both CNTs (h) and CNFs (j) have been observed at the high temperature growth of 725 °C.

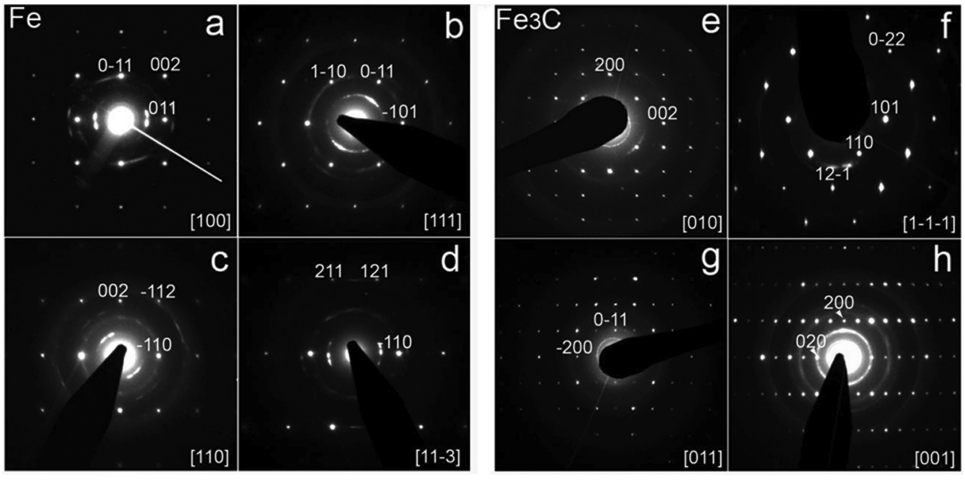


**Figure 3.** Experimental selected-area electron diffraction patterns (EDPs) of the nanoparticle catalysts obtained by tilting them to low index zone axes. (a) [100], (b) [111], (c) [110], and (d) [11$\bar{3}$] EDPs of Fe; (e) [010], (f) [1$\bar{1}$1], (g) [011], and (h) [001] EDPs of $Fe_3C$ (cementite). $Fe_3C$ catalysts were found at all growth temperatures, whereas Fe catalysts were only found at the relatively higher temperatures of 650 and 725 °C.

of the CNFs grown at 600, 650, and 725 °C. As suggested by their dark contrast in the SEM images, all the top parts of CNFs are occupied by nanoparticles, indicating a tip-growth mode, which is anticipated from a dc-PECVD growth technique on a $SiO_2$ substrate (no chemical interaction between catalyst and substrate). Low-magnification TEM images in Figure 2 display the general morphology of CNFs at different growth temperatures, whereas the corresponding enlarged bright-field TEM images emphasize the morphology of the nanoparticle catalysts. Irrespective of the growth temperatures, catalysts show elongated tear-drop shape along CNF axes, which is consistent with the common observation of nanoparticles when CNF growth is performed by CVD.

Selected-area EDPs (Figure 3) were recorded to identify the crystal structure of individual catalyst nanoparticles. Both $\alpha$-Fe (ferrite, BCC, $a$ = 0.287 nm) and $Fe_3C$ (cementite,


dx.doi.org/10.1021/cm202315j | *Chem. Mater.* 2011, 23, 5379–5387

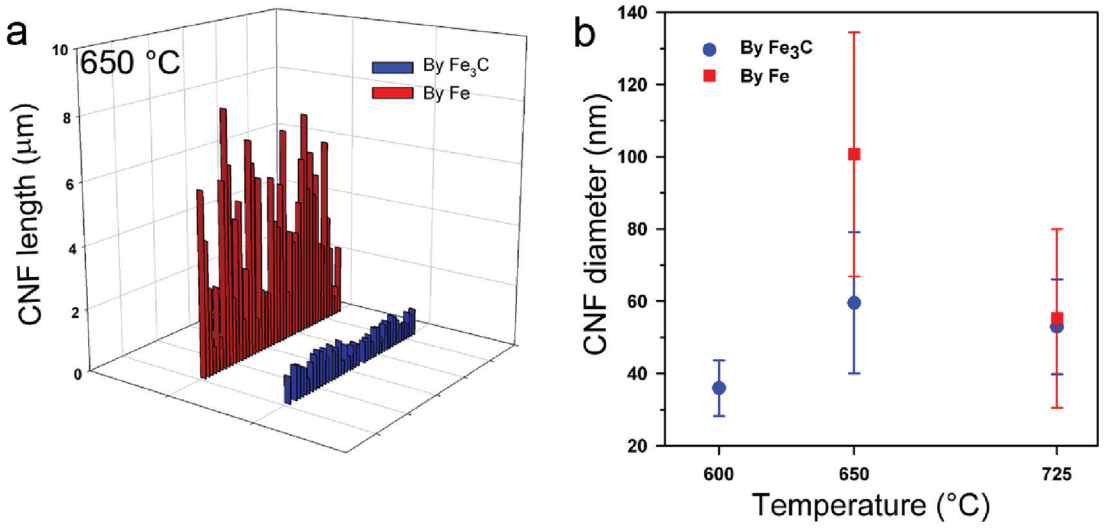


**Figure 4.** Effect of Fe and $Fe_3C$ on the growth of CNFs. (a) Plots of the measured lengths of CNFs catalyzed by Fe and $Fe_3C$ at 650 °C. The length of CNFs was measured by TEM on randomly picked specimens. (b) Spreading of diameter values for CNFs/CNTs catalyzed by Fe and $Fe_3C$ as a function of growth temperatures. Both the averaged values and standard error bars are shown.

orthorhombic, *Pnma* space group, $a$ = 0.509 nm; $b$ = 0.674 nm; $c$ = 0.452 nm) were found to act as catalysts for the growth of CNFs. However, over the 30 fibers that we analyzed here, only $Fe_3C$ was found at the tips of CNFs which were grown at the low temperature of 600 °C. We note that Yoshida et al., also found $Fe_3C$ at the growth temperature of 600 °C,[4] even though using different growth conditions and particle size, leading to CNT growth (as opposed to CNF). In contrast, both $\alpha$-Fe and $Fe_3C$ were observed at the higher growth temperatures of 650 and 725 °C (see the Supporting Information, Table 1). At 650 °C, over the collection of nanoparticles examined, we found 42 $Fe_3C$ and 80 Fe particles (i.e., 34.4% of $Fe_3C$), whereas at 725 °C, there are 50 $Fe_3C$ and 106 Fe particles (i.e., 32% $Fe_3C$). There is thus a threshold temperature for the occurrence of $\alpha$-Fe nucleation, with no appearance below 600 °C (we confirmed this with an experiment at 575 °C, which only shows $Fe_3C$), and a slowly varying existence at higher temperature.

**3.2. Shape of Catalyst Nanoparticles and Nanofiber Structure.** Interestingly, two distinct kinds of morphologies of nanoparticles, namely rounded head (Figure 2k) and faceted head (Figure 2l), are found to be closely correlated with the catalysts' crystal structures determined from the analysis of EDPs. Those catalysts with faceted heads are $\alpha$-Fe (Figure 3a–d), whereas those having round heads are primitive orthorhombic $Fe_3C$ (Figure 3e–h). Furthermore, some correlations between the phases of nanoparticle catalysts and the CNF structure are also found. CNFs catalyzed by $Fe_3C$ at 650 or 725 °C always exhibit a bamboo-like morphology, with thick compartment-separating joints encapsulated quasi-periodically in the CNF hollow core (Figure 2e, j, blue arrowheads; see the Supporting Information, Figures S4 and S5). Inversely, only few random graphene layers are found in the CNF core when growth is catalyzed by $\alpha$-Fe. Surprisingly, the percentage of the bamboo-like CNFs catalyzed by $Fe_3C$ is 100%, found by checking more than 40 bamboo-like CNFs at each temperature of 650 and 725 °C, where Fe and $Fe_3C$ coexist. In other words, no CNFs catalyzed by Fe have a bamboo-like structure with the thick compartment-separating joints in their hollow cores. It is worth pointing out that the enlongated $\alpha$-Fe nanoparticle tails observed at a relatively high temperature (725 °C) drive the walls of CNFs parallel to their growth axis (Figure 2g, h and the Supporting Information, Figure S5e, f), so that the CNFs then become true carbon nanotubes according to the definitions in ref 2.

**3.3. CNF Size Depending on the Type of Catalyst (Fe or $Fe_3C$).** The simultaneous occurrence of Fe and $Fe_3C$ at 650 and 725 °C gives us the opportunity to directly compare the growth rates of CNFs/CNTs which are grown under exactly the same synthesis conditions. The length of CNTs/CNFs is an important parameter because we are mainly interested in field emission applications, and the field amplification factor, $\beta$, at the tip of a needle-like field emitter can be expressed as $\beta \approx L/r$, where $L$ is the length of the needle and $r$ is the radius of curvature at its tip.[24] Figure 4a displays the length of CNFs catalyzed at 650 °C by Fe and $Fe_3C$, respectively. Although the CNFs might have been broken during the TEM sample preparation when scratching them from the growth substrate, the probability for breakage is similar for all fibres, meaning that the striking difference in the relative lengths of CNFs catalyzed by Fe and $Fe_3C$ is certainly significant. Said differently, we believe that CNFs detach from the substrate at their roots upon scratching. For the collection of specimens examined here, the longest CNF catalyzed by Fe is 8.15 $\mu$m, which is 6.8 times as large as the longest CNF grown from $Fe_3C$ (1.20 $\mu$m). The average length of CNFs catalyzed by Fe is 4.6 times larger than that of CNFs grown by $Fe_3C$ (3.91 $\mu$m versus 0.85 $\mu$m). The obvious discrepancy in the length of CNFs grown by Fe and $Fe_3C$ was also found in the samples synthesized at 725 °C although with a factor of ~3 between the two average sizes (see the Supporting Information, Figure S6).

The average diameters of CNFs catalyzed by Fe and $Fe_3C$ as a function of growth temperatures are plotted in Figure 4b for comparison. The largest diameters of CNFs grown by Fe and $Fe_3C$ at 650 °C are 162 and 97.6 nm, respectively. The average diameter of CNFs grown from Fe nanoparticles at 650 °C is 100.7 nm, which is 1.69 times larger than the diameter of CNFs grown from $Fe_3C$ nanoparticles (59.5 nm) under the same conditions. This is directly related to the significantly larger size (on average) of the $\alpha$-Fe particles compared to the $Fe_3C$ ones at 650 °C (see Figures 2d and e). However, the average diameter of CNFs grown from Fe catalysts at 725 °C is almost


dx.doi.org/10.1021/cm202315j | *Chem. Mater.* 2011, 23, 5379–5387

the same as that of $Fe_3C$-grown CNFs at 725 °C (55.3 nm versus 53.0 nm). In other words, the average diameter of CNFs grown by Fe decreases drastically (from 100.7 to 55.3 nm) when the temperature increases from 650 to 725 °C, whereas no significant difference can be observed in the case of $Fe_3C$ nanoparticles. Furthermore, the distribution of CNF diameters catalyzed by Fe is wider than that of $Fe_3C$-catalyzed CNFs (Figure 4). As far as field-emission characteristics are concerned,[24] the field amplification factor for Fe-catalyzed fibres, $\beta_{Fe} \approx L_{Fe}/r_{Fe}$, is always larger than the corresponding one for $Fe_3C$-catalyzed fibres.

**3.4. Connections between Graphene Layers and the Catalyst Atomic Planes.** HREM images in Figure 5 show the details of the interface between the Fe catalyst and the graphene layers. Although the side surface of catalyst which serves for the nucleation of graphene layers is conical in shape, with no clear faceting, it is important to image the crystal planes to understand the atomic mechanisms of growth. The viewing direction of Fe in Figure 5 is along the [111] crystallographic direction. The upper graphene layers of CNFs are parallel in this projection to $(\bar{1}\bar{4}\bar{3})_{Fe}$, which is just an indication that the Fe surface has a high energy there, with no minimization by faceting. However, their bending at the connection with the catalyst "shoulder" (yellow arrow in Figure 5b) clearly indicates a specific relationship with the family of Fe planes that emerge at that Fe surface, i.e. $(01\bar{1})_{Fe}$, which are the densest in the BCC structure. Thus the graphene layers are in the continuity of, and appear generated by, the densest planes in the Fe structure. Because of the mismatch between the spacing of graphene layers (0.34 nm) and that of iron $(01\bar{1})$ crystallographic planes (0.20 nm), the interface is at an angle that optimizes the match, so as to maximize the connection of CNF layers with the step edges formed by the intersection of the $(01\bar{1})_{Fe}$ crystallographic planes with the catalyst surface.

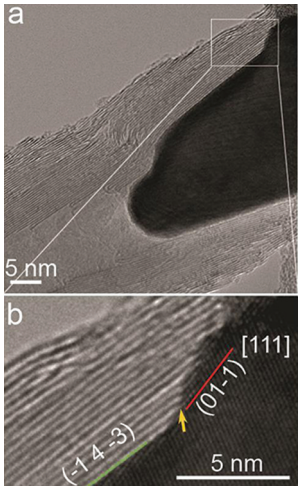


**Figure 5.** HREM images of the interface of graphene layers and Fe catalyst (growth was performed at 725 °C). The boxed area of a is enlarged in b showing more details of the connection area between the graphene layers and $(111)_{Fe}$.

The picture is quite different in the case of $Fe_3C$ catalyst nanoparticles, which exhibit in general smooth side surfaces under a low magnification and do not show large collections of step edges as observed previously on the side surface of Fe nanoparticles. Figure 6 shows the interface between a $Fe_3C$ particle and graphene layers grown at 600 °C: some monatomic steps and protrusions with few atomic steps can be detected at close inspection. This is highlighted on the locations marked by black lattice spots in Figure 6a, two of them being enlarged in Figure 6b, c for more details. Three graphene layers labeled "1", "2", and "3" in Figure 6a are the inner layers of the CNF, as indicated by the blue, red, and green dotted lines, respectively. Layer "1" is discrete, but all its segments connect entirely with the $Fe_3C$ catalyst; layer "2" looks more continuous than layer "1", but more disrupted than layer "3". Layer "3" is the most continuous one among them, with its part connecting with the lower section of the side surface of $Fe_3C$ particle, as seen at the low right-end side in Figure 6a.

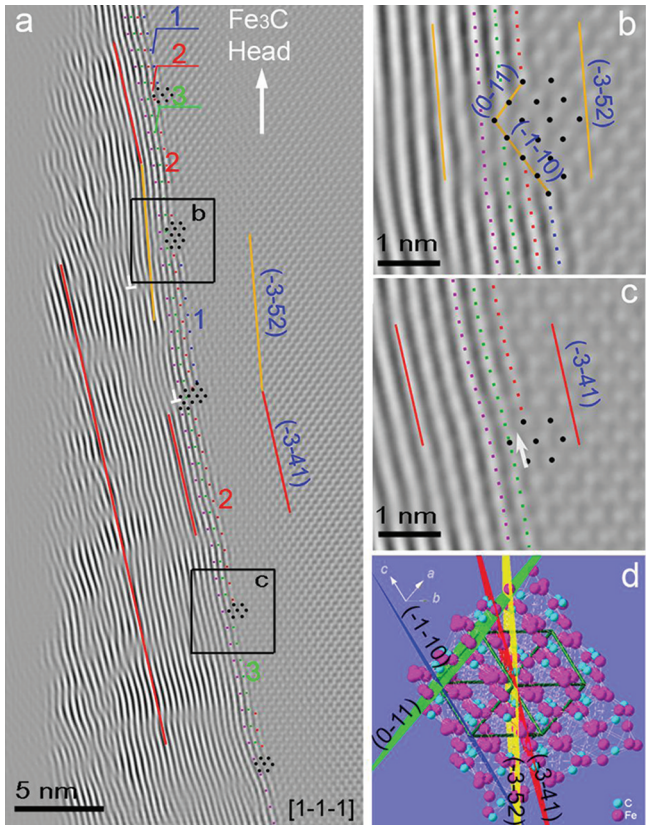


**Figure 6.** Fourier-filtered HREM images of the interface of graphene layers and $Fe_3C$ catalyst (growth was performed at 600 °C). (a) The inner three layers of graphene are connected to the atomic step edges of $Fe_3C$ totally (layer 1) and partially (layers 2 and 3). The discrete distribution of layers implies the multiposition nucleation of graphene layers on the side surface of $Fe_3C$. Here, the graphene layers are mainly parallel to the $(\bar{3}41)$ crystallographic plane of $Fe_3C$. (b-c) Magnified images corresponding to the black frames in a. (d) Atomic projection of $Fe_3C$ along the $[1\bar{1}1]$ direction, with each of the $(0\bar{1}1)$, $(\bar{1}10)$, $(\bar{3}52)$, and $(\bar{3}41)$ crystallographic planes shown.

As with Fe, the graphene layers follow the curvature of the sidewalls of the $Fe_3C$ catalyst particles. For instance, in the TEM image of Figure 6, a majority of graphene layers from the CNF are parallel to the $(\bar{3}41)$ crystallographic plane of $Fe_3C$, with fewer parallel to $(\bar{3}52)$. Again, this is an indication of the high catalyst surface energy needed for graphene nucleation. The deviation of the orientation of the graphene layers, caused by the change of the crystallographic side surface of the elongated convex $Fe_3C$ particle, is compensated by inserting some more graphene layers, hence the presence of edge-type dislocations, marked by a white "⊥" in Figure 6a.


dx.doi.org/10.1021/cm202315j | Chem. Mater. 2011, 23, 5379–5387

Another reason for the generation of dislocations in the CNF structure would be the nucleation at multipositions. The number of atomic steps on the $Fe_3C$ side wall varies depending on the nucleation location, e.g., 2 and 3 graphene layers at the up- and down-sides of the protrusion in Figure 6b, and only one in Figure 6c. The merging of different numbers of graphene layers spreading from different nucleation sites could misfit, which induces one more graphene layer to be inserted between two continuous graphene layers leading to an edge dislocation, as seen in Figure 6a.

## 4. DISCUSSION

Quite generally, plasma-enhanced catalytic chemical vapor deposition proceeds in two steps: first, an annealing step, during which the catalytic material, which is a continuous film at the beginning of the process, looses its integrity upon heating and breaks up (a process driven by the reduction of the surface/interface energy of the system), forming aggregates that start dissociating carbon molecules and accumulating carbon atoms; and a second step, where the actual growth of carbonaceous nano-objects takes place by precipitation of the excess carbon from the supersaturated nanoaggregates. The present observations thus bring two kinds of information: (1) during the first stage, the iron may transform completely into cementite at 600 °C, but not completely at 650 and 725 °C (as explained in the following paragraph, we exclude a transformation during cooling after growth); and (2) when both Fe and cementite have formed, CNFs grow much faster with Fe than with cementite during the second stage.

**4.1. Cementite: Formed after or before the Cooling Stage?** There is a question about when $Fe_3C$ is generated: is it formed during the first stage of the synthesis process and maintained during the growth of CNFs or is it formed during the cooling down process after PECVD growth? It is quite difficult to answer this question unless in situ observations on the crystal structure of the nanoparticles during the PECVD growth process are performed. However, we speculate that the Fe → $Fe_3C$ transformation is impossible after growth, based on the following arguments. First, there are two different kinds of structures of CNFs, as shown in Figure 2 (and discussed above), which strongly suggests that the catalysts at the time of growth are probably different. As quoted above, EDPs clearly show that depending on the CNF structure, the catalysts are Fe or $Fe_3C$. In other words, the differences of catalyst types can explain the difference of the CNF structures and we cannot figure out how the whole CNF structure would change during cooling. Second, because of the large difference of CNFs' length (and thus growth rate) depending on whether we find Fe or $Fe_3C$ at their tips, we can only assume that the iron or carbide observed after growth were indeed present during growth, and even that they had formed before actual growth, during the incubation stage. Third, as summarized in Figure 2 and already discussed, the shape of Fe and $Fe_3C$ nanoparticles is drastically different. It is also hard to figure out how (i) the facets of the Fe nanoparticles' growth front can be transformed into the round surface of $Fe_3C$ upon cooling, and (ii) how the large collection of growth steps at the side surface of these Fe nanoparticles would disappear after the growth process, still during the cooling stage. Therefore, we think that $Fe_3C$ nanoparticles were formed during the first stage of growth (annealing) and kept as catalysts during the growth process, which is also suggested by the uniform structure of CNFs grown by $Fe_3C$, e.g., the thick compartment-separating joints encapsulated quasi-periodically in the CNF hollow core, as seen in Figures S4b−d and S5c in the Supporting Information. Note, for instance in Figure S4d, that the thick compartments inside the fiber can be seen right from the bottom part, which tells us that $Fe_3C$ was already there at the beginning of growth. In fact those compartments can be used as a marker for growth from $Fe_3C$.

**4.2. Iron or Carbide?** A quick look at the Fe−C phase diagram tells us that under the eutectoic temperature (∼ 730 °C), the only phases are $\alpha$-Fe and graphite. The $Fe_3C$ domain of existence consists in a vertical straight line, indicating that this compound supports very little off-stoichiometry. As carbon solubility is well below 0.1 at % in $\alpha$-Fe,[25] $Fe_3C$ or graphite should appear as soon as the carbon concentration reaches a few fractions of percent in iron. Carbon solubility in $\alpha$-Fe in the 600−700 °C range is slightly higher when the solution is in equilibrium with cementite[25,26] than with graphite, which indicates that graphite − and not cementite − should precipitate first from an iron solution that becomes supersaturated with carbon. However, what differentiates the appearance of one of the two phases is more probably related to the parameters classically involved in heterogeneous nucleation: surface energy, elastic energy, and density of nucleation sites.

An incubation period is necessary before the onset of graphene nucleation.[4,27] During this incubation time, carbon invades the $\alpha$-Fe catalyst seeds very rapidly, as carbon diffusion is very fast in $\alpha$-Fe (see our discussion on growth rate below), thus reaching almost instantaneously the solubility limit. The carbon then has to precipitate, either directly in the form of graphite (or rather graphene sheets), or in the form of carbide. Graphene is two-dimensional in nature, with very low surface energy (46.7 $mJ/m^2$, see ref 28), so that its precipitation cost at the surface of nanoparticles is low, except at the nucleation stage, where the proportion of lateral − high-energy − surfaces or edges remains significant (e.g., Figure 5). Thus the occurrence of graphene essentially depends on the density and quality of nucleation sites on the nanoparticles. Cementite has in contrast a standard 3D structure, related to that of $\alpha$-Fe,[29] but with quite different crystal symmetries and lattice parameters. Thus its precipitation costs in an iron matrix have to include significant interface and elastic energy terms. In other words, once $Fe_3C$ is locally nucleated, the $Fe_3C$−Fe interface has to progress inside the Fe particle (overcoming interface energy and elastic energy barriers) until the latter has completely turned into cementite. This will tend to occur in smaller particles, because the interface has less to travel, which is consistent with what we observe at 650 °C (see Figure 2d, e). On the other hand, as the growth temperature is raised, the number of vacancies in $\alpha$-Fe increases, which tends to ease the self-diffusion of Fe atoms, favoring the formation of atomic steps on the side walls of the nanoparticle (inducing reshaping of the particle) and thus favoring the nucleation of graphene layers. So, our understanding is that at low growth temperature (600 °C and below), the reshaping of the Fe catalyst particle (leading to step formation and graphene precipitation) is not fast enough to overtake nucleation and growth of $Fe_3C$, whereas at higher temperature, the two mechanisms coexist, resulting in mixtures of Fe and $Fe_3C$ catalysts.

The question now is how general are the present results and observations? Of course our growth conditions are rather specific, but we note that Behr and co-workers[30] have also found mixtures of Fe and $Fe_3C$ in their nanotubes/nanofibers,

grown by PECVD at 800 °C, even though they used inductive coupling (ICP) for plasma excitation and they observed root-growth conditions because their iron catalysts interact with the Si substrate. They attributed the difference in catalyst structure to the growth atmosphere ($H_2$ partial pressure), which obviously is not the main parameter to consider, since here we observe mixtures of Fe and $Fe_3C$ without changing the growth atmosphere. Also, de Resende and co-workers[21] find the simultaneous occurrence of $\alpha$-Fe and $Fe_3C$ (as well as $\gamma$-Fe) at 1025 °C growth temperature, using pure CVD. Anisimov and co-workers[13] found $Fe_3C$, in conjunction with Fe, although in their growth conditions (CO disproportionation between ~850 and 1050 °C and very small residence time in the furnace), they observed $Fe_3C$ to be inactive for CNT growth. So, whatever the mechanism, this phenomenon of simultaneous occurrence of Fe and $Fe_3C$ is seen in other reports, for growth temperatures above 600 °C, but has never been systematically studied. On the other hand, as already quoted, Yoshida and co-workers (ref 4) have found only $Fe_3C$ at 600 °C, consistently with our observations.

**4.3. Growth Rate.** Now that we have qualitatively explained the presence or absence of metal or carbide with nucleation barrier considerations, we shall see that the different growth rates (in our 650 and 725 °C growth treatments) stem additionally from other parameters. Depending on the process parameters, the growth of CNTs can be limited by (i) nucleation,[31] (ii) carbon diffusion inside[4,32] or at the surface of the catalyst[33,34] and (iii) feedstock supply,[35] including adsorption and dissociation of the gas molecules or radicals on the surface of the catalyst particles.

Let us first examine the diffusion of carbon atoms across the nanoparticles. The diffusion coefficient of C in $\alpha$-Fe,[36] is much larger than that of C in $Fe_3C$:[37] $D_{Fe}$ (600 °C) = $9 \times 10^{-8}$ $cm^2s^{-1}$ and $D_{Fe}$ (725 °C) = $4 \times 10^{-7}$ $cm^2s^{-1}$ to be compared respectively to $D_{Fe3C}$ (600 °C) = $9 \times 10^{-13}$ $cm^2s^{-1}$ and $D_{Fe3C}$ (725 °C) = $10^{-11}$ $cm^2s^{-1}$. Thus, if one compares the typical diffusion times across the nanoparticle catalysts, e.g., to reach a diffusion length $2(Dt)^{1/2} \approx 10$ nm, for Fe and $Fe_3C$ in the 600–725 °C temperature range, one will count the former in microseconds and the latter in seconds. As moreover, recent studies indicate that for Fe catalyst, C diffusion occurs via a surface or subsurface mechanism[33,34] (which usually is a low energy path compared to bulk diffusion[33]), whereas for $Fe_3C$, carbon would diffuse in the bulk via a vacancy-assisted mechanism,[4] the difference becomes huge.

Thus we infer that the difference of growth rate between the two catalysts is essentially due to the fact that carbon atoms cross the nanoparticles of $\alpha$-Fe and $Fe_3C$ by two different means: fast diffusion of carbon atoms for $\alpha$-Fe, and a slow diffusion of the carbon with a compensating vacancy flux for $Fe_3C$. The fact that the difference in growth rate decreases, when the temperature increases from 650 to 725 °C, is probably due the different activation energies of the two mechanisms (0.86[35] and 1.79 eV,[37] respectively, for carbon diffusion in $\alpha$-Fe and cementite).

Finally, let us also add that the dissociation rate of the carbon-bearing radicals on the surface of the catalyst particles might also be more effective on Fe than on $Fe_3C$, due to the faceting of the leading edge of the Fe nanoparticles (i.e., the side exposed to the growth nutrients). Begtrup and co-workers[34] have recently demonstrated the catalytic effect of Fe-facets in the case of an amorphous feedstock, by both in situ TEM observations and calculations.

**4.4. Mechanisms of Growth: Iron.** Next, we focus on the step-edge sites on the side surfaces of catalysts, which have been ascertained as nucleation centers for CNT growth by in situ as well as postgrowth TEM observations.[38−40] Here, large collections of step edges are generally found at the side surfaces of the head of Fe catalysts, as indicated by red arrowheads in Figure 2 and the Supporting Information, Figure S7. Some graphene layers are found to collectively nucleate under these step edges, e.g. a group of 15 graphene layers as shown in the Supporting Information, Figure S7. We note that large nucleation areas certainly help keeping the carbon concentration low in the catalyst nanoparticle, thus preventing the Fe → $Fe_3C$ transformation as explained above.

Taken altogether, the above observations suggest that the growth mechanisms of graphene layers on Fe would be similar to what has been observed previously on Ni,[7,38] i.e., based on the formation of atomic steps on the lateral walls of the nanoparticles, followed by nucleation of graphene layers and migration of the steps on both sides as graphene extends. Steps accumulate below the leading edge of the Fe particle (resulting in the characteristic "nail head" shape), because (i) they cannot cross the edges toward the front facets as they would have to completely reorganize to do that, and (ii) the step diffusion rate on the facets exposed to the growth nutrients is probably slowed-down by carbon/defect accumulation there. On the other hand, as already suggested above, step diffusion toward the trailing edge results in an elongation of the nanoparticle, thus driving the walls of the nanoparticle more and more parallel to the CNF axis and eventually leading to the growth of nanotubes (see Figure S5e, f in the Supporting Information).

The decrease in diameter of the Fe nanoparticles as the temperature increases is probably the result of a stronger dewetting during the incubation stage of the growth, which leads to smaller nanoparticles. It is worth noting, however, that the elongation mentioned above should be enhanced by increasing temperatures as it depends on surface step mobility, which in turn, should also decrease the particle and CNFs' diameter.

**4.5. Mechanisms of Growth: Cementite.** Although $Fe_3C$ has already been observed as catalyst for the growth of CNFs/CNTs,[4,5,14−19] few works have focused on its growth mechanisms.[41] Recently, $Fe_3C$ was found as catalyst for the base-growth of CNTs by in situ environmental TEM.[4] However, the mechanism for the tip-growth of CNTs/CNFs by $Fe_3C$ catalysts is still scarcely documented. HREM images in Figure 6 give some clues for understanding the growth mechanism of CNFs by $Fe_3C$. The discrete inner layers could imply that the graphene layers catalyzed by $Fe_3C$ nucleate simultaneously at multipositions, where steps are available. Note that the discrete inner graphene layers are always connected to the step edges of $Fe_3C$, which again is similar to what has been observed on nickel using in situ TEM,[38] and confirmed by theoretical calculations.[9,38,42]

The protrusions on the side walls of the $Fe_3C$ catalyst particles could be due to the accumulation of steps having diffused from both sides in order to let the graphene layer grow (again, mechanisms of refs 7 and 38). There are two types of atoms (C and Fe) in atomic steps, which imply a collective diffusion process when the steps move. It is in this process that $Fe_3C$ would loose carbon atoms to the graphite. In a vacancy-assisted mechanism, this would create carbon vacancies in the cementite lattice that would have to migrate to the nanoparticle's surface where the feeding gas is decomposed.


dx.doi.org/10.1021/cm202315j | Chem. Mater. 2011, 23, 5379–5387

## 5. CONCLUSION

We have observed the concomitant growth of CNFs/CNTs from Fe and $Fe_3C$ nanoparticles and confirmed that orthorhombic $Fe_3C$ (cementite) can act as a catalyst for the tip-growth of CNFs/CNTs by PECVD. Furthermore, the different phases of $\alpha$-Fe and $Fe_3C$ nanoparticle catalysts can be controllably varied by adjusting the growth temperatures. At low temperatures (600 °C), only $Fe_3C$ acts as a catalyst for the growth of CNFs. However, both $\alpha$-Fe and $Fe_3C$ (cementite) are active at the higher temperatures of 650 and 725 °C. The growth rates of CNFs/CNTs from Fe and $Fe_3C$ nanoparticles are compared under exactly the same growth conditions: the average length of CNFs grown by Fe is much higher than that of CNFs grown by $Fe_3C$ at both 650 and 725 °C. We also find that the structure of CNFs grown from Fe is markedly different from that of CNFs grown from $Fe_3C$. We have attributed the higher growth rate from Fe nanoparticles to a much faster diffusion of carbon atoms across those particles. Moreover, only Fe nanoparticles at a high temperature of 725 °C are found to catalyze the growth of real carbon nanotubes, where the graphene layers are parallel to the tube axis.

According to our observations, the growth mechanisms of CNFs/CNTs from Fe and $Fe_3C$ can be explained by graphene nucleation at step edges, followed by migration of those step edges, similarly to the observations already made on Ni nanoparticles during the growth of CNFs. However, the steps on the crystallographic planes composing the sidewalls of the $Fe_3C$ nanoparticles include two types of atoms, which slows down their formation and their migration rates compared to Fe. Consequently, the growth front of iron and cementite particles present different shapes: the former being faceted and the latter rounded.

## ■ ASSOCIATED CONTENT

### Supporting Information

Additional figures, table, and information. This material is available free of charge via the Internet at http://pubs.acs.org.

## ■ AUTHOR INFORMATION


### Corresponding Author

*E-mail: hezhanbing@gmail.com (Z.H.); didier53@skku.edu (D.P.).

### Present Address

‡EMAT, University of Antwerp, Groenenborgerlaan 171, Antwerp B-2020, Belgium.


## ■ ACKNOWLEDGMENTS

Z.H. thanks Dr. G. Rizza and P.-E. Coulon at Laboratoire des Solides Irradiés, Ecole Polytechnique, France, for use of the CM 30 microscope. D.P. acknowledges partial support from WCU program, through the NRF of Korea, funded by MEST (R31-2008-000-10029-0). This work has been supported by the Region Ile-de-France in the framework of C'Nano IdF as well by the ANR project "Nanoscanner". C'Nano IdF is the nanoscience competence center of Paris Region, supported by CNRS, CEA, MESR, and Region Ile-de-France.

## ■ REFERENCES


(1) Öncel, Ç.; Yürüm, Y. *Fullerenes, Nanotubes, Carbon Nanostruct.* **2006**, *14*, 17.

(2) Melechko, A. V.; Merkulov, V. I.; McKnight, T. E.; Guillorn, M. A.; Klein, K. L.; Lowndes, D. H.; Simpson, M. L. *J. Appl. Phys.* **2005**, *97*, 041301.

(3) Meyyappan, M. *J. Phys. D: Appl. Phys.* **2009**, *42*, 213001.

(4) Yoshida, H.; Takeda, S.; Uchiyama, T.; Kohno, H.; Homma, Y. *Nano Lett.* **2008**, *8*, 2082.

(5) Homma, H.; Kobayashi, Y.; Ogino, T.; Takagi, D.; Ito, R.; Jung, Y. J.; Ajayan, P. M. *J. Phys. Chem. B* **2003**, *107*, 12161.

(6) Amara, H.; Bichara, C.; Ducastelle, F. *Phys. Rev. B* **2006**, *73*, 113404.

(7) Abild-Pedersen, F.; Norskov, J. K.; Rostrup-Nielsen, J. R.; Sehested, J.; Helveg, S. *Phys. Rev. B* **2006**, *73*, 115419.

(8) Hofmann, S.; Sharma, R.; Ducati, C.; Du, G.; Mattevi, C.; Cepek, C.; Cantoro, M.; Pisana, S.; Parvez, A.; Cervantes-Sodi, F.; Ferrari, A. C.; Dunin-Borkowski, R.; Lizzit, S.; Petaccia, L.; Goldoni, A.; Robertson, J. *Nano Lett.* **2007**, *7*, 602.

(9) Amara, H.; Bichara, C.; Ducastelle, F. *Phys. Rev. Lett.* **2008**, *100*, 056105.

(10) Zhang, X.; Cao, A.; Wei, B.; Li, Y.; Wei, J.; Xu, C.; Wu, D. *Chem. Phys. Lett.* **2002**, *362*, 285.

(11) Park, J.-B.; Choi, G.-S.; Cho, Y.-S.; Hong, S.-Y.; Kim, D.; Choi, S.-Y.; Lee, J.-H.; Cho, K.-I. *J. Cryst. Growth* **2002**, *244*, 211.

(12) Sengupta, J.; Jacob, C. *J. Cryst. Growth* **2009**, *311*, 4692.

(13) Anisimov, A. S.; Nasibulin, A. G.; Jiang, H.; Launois, P.; Cambedouzou, J.; Shandakov, S. D.; Kauppinen, E. I. *Carbon* **2010**, *48*, 380.

(14) Ni, L.; Kuroda, K.; Zhou, L.-P.; Ohta, K.; Matsuishi, K.; Nakamura, J. *Carbon* **2009**, *47*, 3054.

(15) Emmenegger, C.; Bonard, J. M.; Mauron, P.; Sudan, P.; Lepora, A.; Grobety, B.; Züttel, A.; Schlapbach, L. *Carbon* **2003**, *41*, 539.

(16) Nishimura, K.; Okazaki, N.; Pan, L.; Nakayama, Y. *Jpn. J. Appl. Phys.* **2004**, *43*, L471.

(17) Peigney, A.; Coquay, P.; Flahaut, E.; Vandenberghe, R. E.; De Grave, E.; Laurent, C. *J. Phys. Chem. B* **2001**, *105*, 9699.

(18) Oberlin, A.; Endo, M.; Koyama, T. *J. Cryst. Growth* **1976**, *32*, 335.

(19) Behr, M. J.; Mkhoyan, K. A.; Aydil, E. S. *ACS Nano* **2010**, *4*, 5087.

(20) Louis, B.; Gulino, G.; Vieira, R.; Amadou, J.; Dintzer, T.; Galvagno, S.; Centi, G.; Ledoux, M. J.; Pham-Huu, C. *Catal. Today* **2005**, *102−103*, 23.

(21) de Resende, V. G.; De Grave, E.; Cordier, A.; Weibel, A.; Peigney, A.; Laurent, C. *Carbon* **2009**, *47*, 482.

(22) Kim, D.; Lim, S. H.; Guilley, A. J.; Cojocaru, C. S.; Bourée, J. E.; Vila, L.; Ryu, J. H.; Park, K. C.; Jang, J. *Thin Solid Films* **2008**, *516*, 706.

(23) He, Z. B.; Maurice, J.-L.; Lee, C. S.; Gohier, A.; Pribat, D.; Legagneux, P.; Cojocaru, C. S. *Carbon* **2011**, *49*, 435.

(24) Utsumi, T. *IEEE Trans. Electron Devices* **1991**, *38*, 2276.

(25) Hasebe, M.; Ohtani, H.; Nishizawa, T. *Metall. Mater. Trans. A* **1985**, *16*, 913.

(26) Chipman, J. *Metall. Mater. Trans. B* **1972**, *3*, 55.

(27) Le Normand, F.; Švrček, V.; Senger, A.; Dintzer, T.; Pham-Huu, C. *J. Phys. Chem. C* **2009**, *113*, 14879.

(28) Wang, S.; Zhang, Y.; Abidi, N.; Cabrales, L. *Langmuir* **2009**, *25*, 11078.

(29) Sharma, R.; Moore, E.; Rez, P.; Treacy, M. M. J. *Nano Lett.* **2009**, *9*, 689.

(30) Behr, M. J.; Gaulding, E. A.; Mkhoyan, K. A.; Aydil, E. S. *J. Appl. Phys.* **2010**, *108*, 053303.

(31) Page, A. J.; Ohta, Y.; Irle, S.; Morokuma, K. *Acc. Chem. Res.* **2010**, *43*, 1375.

(32) Baker, R. T. K.; Harris, P. S.; Thomas, R. B.; Waite, R. J. *J. Catal.* **1973**, *30*, 86.

(33) Hofmann, S.; Csanyi, G.; Ferrari, A. C.; Payne, M. C.; Robertson, J. *Phys. Rev. Lett.* **2005**, *95*, 036101.

(34) Begtrup, G. E.; Gannett, W.; Meyer, J. C.; Yuzvinsky, T. D.; Ertekin, E.; Grossman, J. C.; Zettl, A. *Phys. Rev. B* **2009**, *79*, 205409.

(35) Hafner, J. H.; Bronikowski, M. J.; Azamian, B. R.; Nikolaev, P.; Rinzler, A. G.; Colbert, D. T.; Smith, K. A.; Smalley, R. E. *Chem. Phys. Lett.* **1998**, *296*, 195.
(36) Homan, C. G. *Acta Metall.* **1964**, *12*, 1071.
(37) Schneider, A.; Inden, G. *Calphad* **2007**, *31*, 141−147.
(38) Helveg, S.; Lopez-Cartes, C.; Sehested, J.; Hansen, P. L.; Clausen, B. S.; Rostrup-Nielsen, J. R.; Abild-Pedersen, F.; Norskov, J. K. *Nature* **2004**, *427*, 426.
(39) Lin, M.; Tan, J. P. Y.; Boothroyd, C.; Loh, K. P.; Tok, E. S.; Foo, Y. −L. *Nano Lett.* **2007**, *7*, 2234.
(40) Zhu, H. W.; Suenaga, K.; Hashimoto, A.; Urita, K.; Hata, K.; Iijima, S. *Small* **2005**, *1*, 1180.
(41) Schaper, A. K.; Hou, H.; Greiner, A.; Phillipp, F. *J. Catal.* **2004**, *222*, 250.
(42) Nørskov, J. K.; Bligaard, T.; Logadottir, A.; Bahn, S.; Hansen, L. B.; Bollinger, M.; Bengaard, H.; Hammer, B.; Sljivancanin, Z.; Mavrikakis, M.; Xu, Y.; Dahl, S.; Jacobsen, C. J. H. *J. Catal.* **2002**, *209*, 275.